Modern Pathology (2021) 34:735–747
https://doi.org/10.1038/s41379-020-00678-6

ARTICLE

Fusion partners of NTRK3 affect subcellular localization of the fusion kinase and cytomorphology of melanocytes

Arnaud de la Fouchardière[1,2] · Meng Kian Tee[3] · Sandra Peternel[4] · Manuel Valdebran[5] · Daniel Pissaloux[1,2] · Franck Tirode[2] · Klaus J. Busam[6] · Philip E. LeBoit[3,7] · Timothy H. McCalmont[3,7] · Boris C. Bastian[3,7] · Iwei Yeh[3,7]

Received: 17 June 2020 / Revised: 21 August 2020 / Accepted: 22 August 2020 / Published online: 23 September 2020

Abstract

A subset of Spitz tumors harbor fusions of *NTRK3* with *ETV6*, *MYO5A*, and *MYH9*. We evaluated a series of 22 melanocytic tumors in which an *NTRK3* fusion was identified as part of the diagnostic workup. Tumors in which *NTRK3* was fused to *ETV6* occurred in younger patients were predominantly composed of epithelioid melanocytes and were classified by their histopathologic features as Spitz tumors. In contrast, those in which *NTRK3* was fused to *MYO5A* were predominantly composed of spindled melanocytes arrayed in fascicles with neuroid features such as pseudo-Verocay bodies. To further investigate the effects of the fusion kinases ETV6-NTRK3 and MYO5A-NTRK3 in melanocytes, we expressed them in immortalized melanocytes and determined their subcellular localization by immunofluorescence. ETV6-NTRK3 was localized to the nucleus and diffusely within the cytoplasm and caused melanocytes to adopt an epithelioid cytomorphology. In contrast, MYO5A-NTRK3, appeared excluded from the nucleus of melanocytes, was localized to dendrites, and resulted in a highly dendritic cytomorphology. Our findings indicate that ETV6-NTRK3 and MYO5A-NTRK3 have distinct subcellular localizations and effects on cellular morphology.

Introduction

Intrachromosomal or interchromosomal rearrangements can fuse receptor tyrosine kinase (RTK) genes with other genes and result in constitutively active oncoproteins that cause neoplasms in different cellular lineages [1]. Approximately 50% of Spitz nevi harbor RTK fusions whereas activating point mutations in BRAF or NRAS are found in the majority of conventional melanocytic nevi [2–8]. Spitz nevi can progress to melanoma by acquisition of additional genetic mutations, and Spitz tumor refers to the entire spectrum from benign Spitz nevi, to intermediate Spitz tumors, to Spitz melanoma. Spitz tumors with intermediate histopathologic features between nevus and melanoma may harbor genetic alterations in addition, such as *CDKN2A* homozygous deletion, and were previously referred to as atypical Spitz tumors. However, the preferred nomenclature for Spitz tumors with more than a single driver event is now Spitz melanocytoma, per the 2018 WHO classification of skin tumors [9]. The nature of the RTK involved in the oncogenic gene fusion found in Spitz tumors can affect their histopathologic features. Spitz tumors with *ALK* fusions have large fascicular nests of melanocytes whereas those with *NTRK1* fusions often have rosette-like structures, filigree-like rete ridges, and exaggerated maturation [10–13].

NTRK3 encodes the tropomyosin receptor kinase TrkC, a member of the neurotrophic tyrosine receptor kinase (NTRK)

✉ Iwei Yeh
Iwei.Yeh@ucsf.edu

1 Department of Biopathology, Center Léon Bérard, Lyon, France
2 Université de Lyon, Université Claude Bernard Lyon 1, INSERM 1052, CNRS 5286, Centre Léon Bérard, Cancer Research Center of Lyon, Equipe Labellisée Ligue contre le Cancer, Lyon, France
3 Department of Dermatology, University of California San Francisco, San Francisco, CA, USA
4 Department of Dermatovenereology, Faculty of Medicine, University of Rijeka, Rijeka, Croatia
5 Department of Dermatology and Dermatologic Surgery, Medical College of South Carolina, Charleston, SC, USA
6 Department of Pathology, Memorial Sloan Kettering Cancer Center, New York, NY, USA
7 Departments of Dermatology and Pathology, University of California San Francisco, San Francisco, CA, USA

family, whose activation mediates neuronal differentiation and survival [14]. It is expressed at low levels in melanocytes [15]. We previously described *NTRK3* fusions in melanocytic tumors with varying N-terminal fusion partners, including *ETV6*, *MYO5A*, and *MYH9* [4]. *NTRK3* fusions are also present in over 50% of pigmented spindle cell nevi of Reed [6]. *NTRK3* fusions, commonly *ETV6-NTRK3* fusions, are further found in other tumor types, including secretory breast carcinoma, mammary analogue secretory carcinoma of the salivary gland, thyroid carcinoma, infantile fibrosarcoma, and congenital mesoblastic nephroma [16–23]. By contrast, *MYO5A-NTRK3* and *MYH9-NTRK3* are so far unique to melanocytic tumors. *MYO5A* encodes myosin Va, a motor protein that moves processively along actin filaments to transport melanosomes [24]. Notably, germline loss of function mutations in *MYO5A* results in the autosomal recessive condition Griscelli syndrome that is characterized by pigmentary dilution [25].

In this study, we describe the different histopathologic features of melanocytic tumors with *ETV6-NTRK3* and *MYO5A-NTRK3* and their different subcellular localizations and effects on melanocyte morphology in vitro.

Materials and methods

Case selection

In addition to 8 cases that we previously reported [14], we identified 14 additional cases with *NTRK3* rearrangement. Ten cases from the Dermatopathology Section of the Departments of Dermatology and Pathology at the University of California, San Francisco had a relative copy number increase of 3′ end of *NTRK3* along with the 5′ portion of one of the known *NTRK3* fusion partners *ETV6*, *MYO5A*, or *MYH9* by array comparative genomic hybridization (aCGH) that was performed for diagnostic purposes. Four cases from the Department of Biopathology at the Centre Léon Bérard in Lyon, France were identified by RNA sequencing which revealed an in-frame fusion of the *NTRK3* mRNA. After review of histopathologic and molecular findings a consensus diagnosis was assigned (IY, AF, SP). Individual histopathologic features were scored by at least two authors (IY, SP, and MV). The study was approved by the human research ethics committees of the Centre Léon Bérard (L17-73) and UCSF (11-07922) and was conducted according to the Declaration of Helsinki.

Array comparative genomic hybridization (aCGH)

Tumor tissue was microdissected from 20-µm-thick sections of formalin-fixed paraffin-embedded (FFPE) tissue. After deparaffinization, DNA was obtained by phenol/chloroform extraction. Array CGH was performed on Agilent 4x180k microarrays (Agilent, Santa Clara, CA, p/n G4449A) according to the manufacturer's instructions. Commercially available normal human DNA (Promega, city, WI, p/n #G1471 or #G1521,) was used as a reference. The raw microarray images were processed with Agilent Feature Extraction software and analyzed with Nexus Copy Number Software version 7.0 (Biodiscovery, El Segundo, CA, USA) as described previously [14].

RNA sequencing

Total RNA was extracted from FFPE tissue sections using a single phenol/chloroform extraction protocol with Trizol reagent (Invitrogen, Carlsbad, CA, USA). RNase-free DNase set (Qiagen, Courtabouef, France) was used to remove DNA. The DNase was eliminated by a second Trizol extraction. RNA was quantified by NanoDrop (Thermo Fisher Scientific, Cheshire, UK) and quality was controlled (DV200 value cutoff >13%) by TapeStation with Hs RNA Screen Tape (Agilent, Courtaboeuf, France).

For each sample, 100 ng of total RNA was used to prepare libraries with the TruSeq RNA Access Library Prep Kit (Illumina, San Diego, USA). Fourteen libraries were pooled at a DNA concentration of 4 nM with 1% PhiX. Sequencing was performed (75 cycles paired end) with the NextSeq 500/550 High Output V2 kit on a NextSeq 500 instrument (Illumina). Data analysis was performed on BaseSpace Sequence Hub (Illumina) with the RNA-Seq Alignment application. Alignments to the human reference genome (hg19) were performed with STAR [26] and TopHat2 [27]. Fusion transcripts were identified with Manta [28] and TopHat2 fusion.

Generation of immortalized melanocytes stably transduced with NTRK3 fusion genes

Using the *NTRK3* fusion constructs generated in our previous study [4], we generated *ETV6-NTRK3* and *MYO5A-NTRK3* fusion constructs in the QM513 cumate inducible lentivirus vector (System Biosciences, catalog number QM513B-1) tagged with the V5 epitope at the carboxyl end.

Melan-a cells (generously provided by Dr Dorothy C. Bennett, St. George's Hospital, University of London, London, UK) [29] were maintained in glutamine-containing RPMI-1640 supplemented with 10% heat-inactivated fetal bovine serum, 200 nM of 12-O-tetradecanoylphorbol-13-acetate, penicillin (100 units/mL), and streptomycin (50 mg/mL). Lentiviral particles were generated in 293FT cells purchased from Life Technologies and maintained in DME-H21 medium containing 10% heat-inactivated fetal bovine serum, minimal essential media nonessential amino acids (0.1 mM), sodium pyruvate (1 mM), penicillin (100 units/mL), and streptomycin (50 mg/mL). Lentiviral transduction

of melan-a cells stably expressing the cumate repressor was performed in the presence of 10 µg/ml of polybrene (Santa Cruz Biotechnology), and the cells were selected by puromycin. After 3 weeks, the cells were subjected to clonal selection by single cell dilution, and clones were expanded in T25 flasks. Cells were grown on cover slides and induced with either 30 or 300 mM cumate for 4 days. Immunofluorescence was done using an anti-V5 antibody primary antibody (Cell Signaling, #13202) and Alexa Fluor 555-nm secondary antibody (Thermo Fisher, #A32732) and DAPI mounting medium (Life Technologies Corporation, #P36931). Fluorescent and differential interference contrast images were captured on a Yokogawa CSU-22 spinning disk confocal microscope with the Nikon Elements software.

Western blotting

Melan-a cells in serum-free media, were lysed with RIPA buffer in the presence of Halt protease and phosphatase inhibitor. Twenty microgram of cell lysates were loaded onto 4–12% Bis-Tris NuPage gradient gels (Life Technologies). Bands were detected by Luminata enhanced chemiluminescence solution (Millipore) followed by autoradiography. The following antibodies were used: anti-pan NTRK (C17F1), anti-phospho-ERK (Thr202/Tyr204) (#9101), anti-phospho-AKT (Ser473) (#9271), and anti-phospho-PLCγ1 (Tyr783) (#2821) from Cell Signaling Technology; and anti-HSP60 (sc-1722) from Santa Cruz Biotechnology.

Immunohistochemistry

Anti-Pan-TRK antibody (Abcam; [EPR17341]) immunohistochemistry was performed on 4-µm sections obtained from FFPE tissues on a Ventana BenchMark ULTRA system (Ventana, Tucson, USA) with the Enhanced Alkaline Phosphatase Red Detection Kit (Ventana; #800–031).

Statistical analysis

Fisher's exact test was used to calculate the significance of differences in characteristics between *ETV6-NTRK3* and *MYO5A-NTRK3* fused tumors. T-test was used to determine if the difference in ages between these two groups was significant.

Results

Clinical characteristics of NTRK3-fused melanocytic tumors

A total of 22 cases for which molecular analysis was performed for diagnostic purposes were included in the study and their clinical features are summarized in Table 1. *MYO5A-NTRK3* was identified in thirteen (59%), *ETV6-NTRK3* in seven (32%), and *MYH9-NTRK3* in two cases (9%). The median age of patients was 20 years, ranging from 1 to 74 years. Nine patients (41%) were age 10 years or younger. There was a slight, but statistically insignificant, predominance of female over male patients (13 and 9, respectively). Half of the tumors ($n = 11$) were located on the head, whereas the remaining tumors were distributed on the trunk ($n = 6$, 27%) and extremities ($n = 5$, 23%). Thirteen tumors (59%) were >5 mm in diameter, and 3 (14%) were >1 cm in diameter. In addition to melanocytic tumors, the initial clinical diagnoses included hemangioma, xanthogranuloma, mastocytoma, basal cell carcinoma, pyogenic granuloma, wart, cyst, and pilomatricoma.

By histopathology, three (14%) cases were diagnosed as benign melanocytic nevus and four (18%) cases as melanoma. Two-thirds of the tumors (15 lesions, 68%) were assigned an intermediate or uncertain diagnosis of atypical Spitz tumor. In two cases (two atypical Spitz tumors and two melanomas), we observed at least one chromosome with multiple alternations between 2–3 copy number states consistent with chromothripsis [30]. The number of atypical Spitz tumors and melanomas reflects the selection for diagnostically challenging cases. Clear cut melanomas that would not require molecular assessment were not included. Molecular assessment played a significant role in the final diagnosis of the cases, and we did not identify histopathologic features that clearly distinguished Spitz melanocytomas from Spitz melanoma in our small cohort. In addition to the chromosomes harboring the genes involved in the *NTRK3* fusion, additional gains and/or losses on other chromosomes were present in 6 of 15 atypical Spitz tumors and in 3 out of 4 melanomas.

Sentinel lymph node biopsy was performed on one child with an atypical Spitz tumor with *ETV6-NTRK3* fusion and revealed a tumoral deposit in a single lymph node. No involvement of additional lymph nodes was found upon completion lymphadenectomy and the patient was alive and well 6 years after diagnosis. Long-term follow-up information was available for five additional patients, including for one patient with melanoma, and was uneventful for local recurrence or metastatic disease.

Tumors with *ETV6-NTRK3* fusion occurred in younger patients as compared to tumors with *MYO5A-NTRK3* fusion ($p < 0.001$, *t*-test) and tended to occur more often on the face (n.s. $p = 0.06$, Fisher's exact test) (Fig. 1). Most of the patients with *MYO5A-NTRK3* fusions were diagnosed between 20 and 50 years of age ($n = 9$, 69%) and had their tumors on the trunk or extremities ($n = 9$, 69%). One patient with *MYO5A-NTRK3* tumor was 72 years old but reported to have had the lesion for over 30 years.

Table 1 Clinicopathologic and genetic features of melanocytic tumors with *NTRK3* fusion.

Case	Age (years), sex	Location	Clinical description	Thickness (mm)[a]	Diameter (mm)[a]	Diagnosis (category)	Clinical follow-up	Studies performed	Copy number aberrations	*NTRK3* fusion partner gene
1[b]	2, F	Shin	7 × 6-mm pink nodule, possible Spitz nevus or juvenile xanthogranuloma or mastocytoma	>1.5	6.0	Spitz nevus	NA	aCGH, RNA-Seq	Gain of 12p (distal to *ETV6*) loss of distal 15q (distal to *NTRK3*)	*ETV6*
2[b]	10, M	Cheek	Pilomatricoma?	4.2	4.7	Spitz nevus	NA	aCGH, RNA-Seq	Small loss near *NTRK3*, no broad/arm-level losses or gains	*MYH9*
3	45, F	Nose	Basal cell carcinoma	>1.4	3.6	Spitz nevus	NA	aCGH	Gain of 15q between *MYO5A* and *NTRK3*	*MYO5A*
4	2, M	Cheek	Growing pink papule, Spitz nevus, juvenile xanthogranuloma, pyogenic granuloma, wart	>3.7	7.3	Spitz melanocytoma (atypical Spitz tumor)	NA	aCGH	Gains of 12p (proximal to *ETV6*), gain of 15q (proximal to *NTRK3*) loss of 15q (distal to *NTRK3*)	*ETV6*
5	5, F	Cheek	Atypical nevus, concern for malignancy	2.6	6.7	Spitz melanocytoma (atypical Spitz tumor)	NA	aCGH	Gain of 5q, loss of distal 13q, gain of 15q between *MYO5A* and *NTRK3* with alternating copy number state in gained segment suggestive of chromothripsis	*MYO5A*
6[b]	6, F	Cheek	Spitz nevus, keratotic nevus, verruca vulgaris	2.6	2.5	Spitz melanocytoma (atypical Spitz tumor)	SLNB with deposit in 1/2 nodes. Completion lymphadenectomy with 0/33 nodes involved. No recurrence (6 years)	aCGH, RNA-Seq	Loss of 15q (distal to *NTRK3*), loss of portions of proximal 7q, loss of proximal 12q, loss of distal 18q	*ETV6*
7[b]	7, M	Cheek	Not available	1.5	4.4	Spitz melanocytoma (atypical Spitz tumor)	NA	aCGH, RNA-Seq	Loss of distal 15q (distal to *NTRK3*), small deletion on 12p involving 3′ end of *ETV6* and deletion of proximal 12q, loss of most of 8p	*ETV6*
8	10, F	Dorsal wrist	Cyst, pilomatricoma?	5.5	5.7	Spitz melanocytoma (atypical Spitz tumor)	NA	aCGH	Gain of proximal 15q proximal to *NTRK3* with high copy gain involving 5′ end of *MYO5A* and 3′ end of *NTRK3*, gain of distal 17q	*MYO5A*
9[b]	10, F	Earlobe	Nevus with central pyogenic granuloma	>1.2	2.9	Spitz melanocytoma (atypical Spitz tumor)	Complete excision, no recurrence (4.5 years)	aCGH, RNA-Seq	Small gain on 15q involving 5′ end of *NTRK3*, gain of distal 12p (distal to *ETV6*), gain of most of 2 (but not distal 2p)	*ETV6*
10[b]	16, F	Scalp	New nevus?	1.5	8.8	Spitz melanocytoma (atypical Spitz tumor)	Complete excision, no recurrence (3 years)	aCGH, RNA-Seq	Multiple losses on 15q with loss of 5′ end of *NTRK3* and deep deletion of 3′ end of *MYO5A* alternating copy number states on 15 suggestive of chromothripsis	*MYO5A*
11	19, F	Ear	Not available	>3	4.0	Spitz melanocytoma (atypical Spitz tumor)	NA	aCGH	Gain of 12p (distal to *ETV6*), gain of 15q (proximal to *NTRK3*)	*ETV6*
12	21, M	Shoulder	Atypical nevus, basal cell carcinoma, amelanotic melanoma	0.7	2.8	Spitz melanocytoma (atypical Spitz tumor)	complete excision, no recurrence (7.5 years)	aCGH	Gain of 15q between *MYO5A* and *NTRK3*, loss of distal 4p, loss of portion of 10q (containing *PTEN*), loss of distal 11q	*MYO5A*
13	36, M	Shoulder	9 × 7-mm variegated deeply pigmented papule	0.7	7.3	Spitz melanocytoma (atypical Spitz tumor)	NA	aCGH	Gain of 15q between *MYO5A* and *NTRK3*	*MYO5A*
14	32, F	Lateral foot	8-mm papule	3.7	6.7	Spitz melanocytoma (atypical Spitz tumor)	NA	RNA-Seq	NA	*MYO5A*
15	38, M	Back	15-mm polypoid nodule	5.7	12.6	Spitz melanocytoma (atypical Spitz tumor)	NA	aCGH, RNA-Seq	Gain of 15q between *MYO5A* and *NTRK3*	*MYO5A*
16[b]	41, F	Trunk	Hemangioma, dysplastic nevus	≥1	6.7	Spitz melanocytoma	NA	aCGH, RNA-Seq	Focal deletions of 15q involving 3′ end of *MYO5A*, 5′ end of *NTRK*3	*MYO5A*

Table 1 (continued)

Case	Age (years), sex	Location	Clinical description	Thickness (mm)[a]	Diameter (mm)[a]	Diagnosis (category)	Clinical follow-up	Studies performed	Copy number aberrations	*NTRK3* fusion partner gene
17	47, F	Back	6 × 3-mm brown exophytic lesion	1.1	3.7	(atypical Spitz tumor) Spitz melanocytoma (atypical Spitz tumor)	NA	RNA-Seq	NA	*MYO5A*
18[b]	72, F	Forehead	Nevus present for 30 years without change	0.9	7.6	Spitz melanocytoma (atypical Spitz tumor)	Complete excision, no recurrence (3 years)	aCGH, RNA-Seq	Loss of 15q proximal to *MYO5A* and distal to *NTRK3*	*MYO5A*
19	1, M	Cheek	3-mm papule, juvenile xanthogranuloma, or Spitz nevus	>1.6	4.5	Melanoma	NA	aCGH	Gain of 15q (proximal to *NTRK3*), loss of distal 15q with alternating copy number states suggestive of chromothripsis, gain of 12p (distal to *ETV6*), loss of 8p, loss of distal 20p, loss of proximal 21q	*ETV6*
20	29, M	Elbow	Cyst, subcutaneous nodule	>5	11.0	Melanoma	NA	aCGH	Gains and losses of 15q with gain of 5′ end of *MYO5A* and loss of 5′ end of *NTRK3* and alternating copy number states suggestive of chromothripsis, gain of distal 2q, small loss and gain on 4p, loss of 8p, losses of 9p with deep deletion of *CDKN2A*	*MYO5A*
21	44, F	Shoulder	15 × 10-mm nodule	8.2	10.3	Melanoma	NA	aCGH, RNA-Seq	Gain of 15q (distal to *MYO5A*) with additional gain if the 3′ end of *NTRK3*, loss of distal 1p, 2q, 7p, and 9q	*MYO5A*
22	74, M	Forearm	Not available	4	7.5	Melanoma	NA	aCGH	Gain of 15q (proximal to *NTRK3*), gain of 22q (distal to *MYH9*)	*MYH9*

aCGH array-based comparative genomic hybridization, *RNA-Seq* transcriptome sequencing.

[a]Maximum value measured in histopathologic sections of the tumor.

[b]Cases included in our earlier report on NTRK3-rearranged Spitz tumors [14].

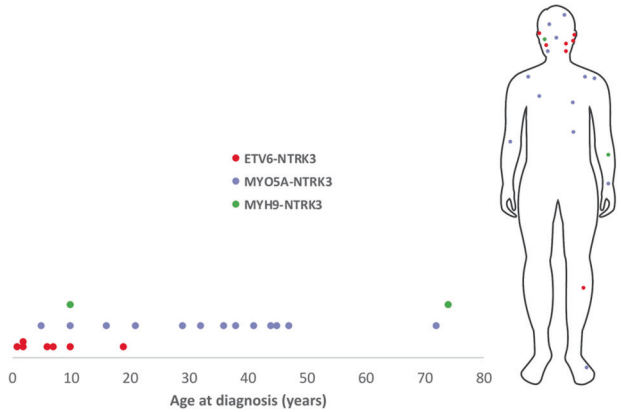

Fig. 1 Age at diagnosis and anatomic distribution of *NTRK3*-fused Spitz tumors. Age and anatomic site distribution for each *NTRK3* fusion partner.

Distinct histopathologic features of melanocytic tumors with ETV6-NTRK3 and MYO5A-NTRK3 fusions

The histopathologic features of *NTRK3*-fused tumors are summarized in Table 2. Most lesions were well-circumscribed, dome-shaped or nodular, dermal or predominantly dermal tumors extending into the reticular dermis. The mean tumor thickness was 2.7 ± 2.02 mm. Of the 16 cases in which the base of the tumor was contained within the biopsy, a majority had a wedge-shaped or bulbous lower contour (56 and 25%, respectively). Most tumors were densely cellular and composed of closely packed nests or interlacing fascicles, some even showing syncytial and sheet-like growth pattern of rather monomorphous melanocytes with minimal intervening stroma. In half, there was poor maturation with descent, while in the other half maturation was limited. The overlying epidermis was thinned in 76%, and ulceration was present in 10%.

The constituent melanocytes had mostly monomorphous rather than pleomorphic features and were occasionally multinucleated. Dermal mitoses were easily detectable in 27%, and if present, were usually scattered throughout the entire tumor rather than limited to superficial portions. One third of all tumors had at least one deep (in the lower third of the tumor) or marginal (within 0.25 mm of the deep periphery of the tumor) mitosis, although this was more commonly observed among tumors with *ETV6-NTRK3* fusion ($p = 0.02$).

In the majority ($n = 6$, 86%) of cases with *ETV6-NTRK3* fusion the predominant morphology of the constituent melanocytes was epithelioid, which was the case in a minority of the *MYO5A-NTRK3*-fused tumors ($n = 5$, 38%), (not significant, $p = 0.07$). *ETV6-NTRK3*-fused tumors often had large coalescing nests, "lobulated nests" similar to those previously described in *NTRK1*-fused tumors [13],

Table 2 Histopathologic features of melanocytic tumors with *NTRK3* fusion.

	NTRK3 fusion subtype by partner gene			
	ETV6	*MYO5A*	*MYH9*	Total
Tumor thickness (mm, mean ± SD)[a]	2.2 ± 0.95	2.9 ± 2.46	4.1 ± 0.15	2.8 ± 2.00
Tumor diameter (mm, mean ± SD)[a]	4.5 ± 1.68	7.2 ± 2.94	6.1 ± 1.98	6.2 ± 2.73
Silhouette				
Dome-shaped	5/7 (71%)	6/13 (46%)	0/2 (0%)	11/22 (50%)
Nodular	2/7 (29%)	4/13 (31%)	1/2 (50%)	7/22 (32%)
Plaque-like	0/7 (0%)	2/13 (15%)	1/2 (50%)	3/22 (13.5%)
Polypoid	0/7 (0%)	1/13 (8%)	0/2 (0%)	1/22 (4.5%)
Flat base[b]	0/4 (0%)	3/10 (30%)	0/2 (0%)	3/16 (19%)
Wedge-shaped base[b]	4/4 (100%)	4/10 (40%)	1/2 (50%)	9/16 (56%)
Bulbous/ dumbbell base[b]	0/4 (0%)	3/10 (30%)	1/2 (50%)	4/16 (25%)
Location of melanocytes				
Compound	2/7 (29%)	4/13 (31%)	0/2 (0%)	6/22 (27%)
Dermal or predominantly dermal	5/7 (71%)	9/13 (69%)	2/2 (100%)	16/22 (73%)
Epidermal changes[c]				
Hyperplasia	3/7 (43%)	2/12 (17%)	1/2 (50%)	6/21 (29%)
Thinned epidermis	7/7 (100%)	9/12 (75%)	0/2 (0%)	16/21 (76%)
Ulceration	2/7 (29%)	0/12 (0%)	0/2 (0%)	2/21 (10%)
Architecture				
Large nests	5/7 (71%)	2/13 (15%)	0/2 (0%)	7/22 (32%)
Back-to-back nests and/or sheets	6/7 (86%)	8/13 (62%)	1/2 (50%)	15/22 (68%)
Fascicles	3/7 (43%)	8/13 (62%)	0/2 (0%)	11/22 (50%)
Pseudo-Verocay bodies	0/7 (0%)	6/13 (46%)	0/2 (0%)	6/22 (27%)
Cytologic features				
Mostly epithelioid	6/7 (86%)	5/13 (38%)	2/2 (100%)	13/22 (59%)
Mostly spindled	1/7 (14%)	8/13 (62%)	0/2 (0%)	9/22 (41%)
Large cells with eccentric nuclei	4/7 (57%)	2/13 (15%)	0/2 (0%)	6/22 (27%)
Multinucleation	4/7 (57%)	5/13 (38%)	1/2 (50%)	10/22 (46%)
Dermal mitoses				
Present	6/7 (86%)	6/13 (46%)	0/2 (0%)	12/22 (55%)
Deep or marginal	5/7 (71%)	2/13 (15%)	0/2 (0%)	7/22 (32%)
Lymphocytic infiltrate				
Throughout the tumor	6/7 (86%)	2/13 (15%)	0/2 (0%)	8/22 (36%)
Patchy at the base/periphery	0/7 (0%)	3/13 (23%)	1/2 (50%)	4/22 (18%)
Other				
Kamino bodies[c]	0/7 (0%)	2/12 (17%)	0/2 (0%)	2/21 (10%)
Pigmentation (moderate to marked)	0/7 (0%)	7/13 (54%)	0/2 (0%)	7/22 (32%)
Maturation (limited)	4/7 (57%)	6/13 (46%)	1/2 (50%)	11/22 (50%)
Sclerotic stroma	1/7 (14%)	8/13 (62%)	2/2 (100%)	11/22 (50%)

[a]For non-excisional biopsies, calculation includes size of the tumor available within a sample.

[b]Includes only cases in which base of the tumor was contained within a biopsy.

[c]Epidermis was missing in one of the samples (case 21).

and sheets of non-maturing melanocytes. Cells were oval to polygonal, with abundant, pale cytoplasm, and large, somewhat pleomorphic, often eccentrically placed nuclei (Fig. 2). Most of the tumors with *ETV6-NTRK3* fusion were composed of melanocytes with glassy cytoplasm and distinct cell borders and a permeating lymphocytic infiltrate, which was observed in only a minority of the cases with *MYO5A-NTRK3* fusion. While none of the tumors with *ETV6-NTRK3* fusion were highly pigmented, considerable significant amounts of melanin were present in slightly more than half ($n = 7$, 53%) of the tumors with *MYO5A-NTRK3* fusion ($p = 0.04$).

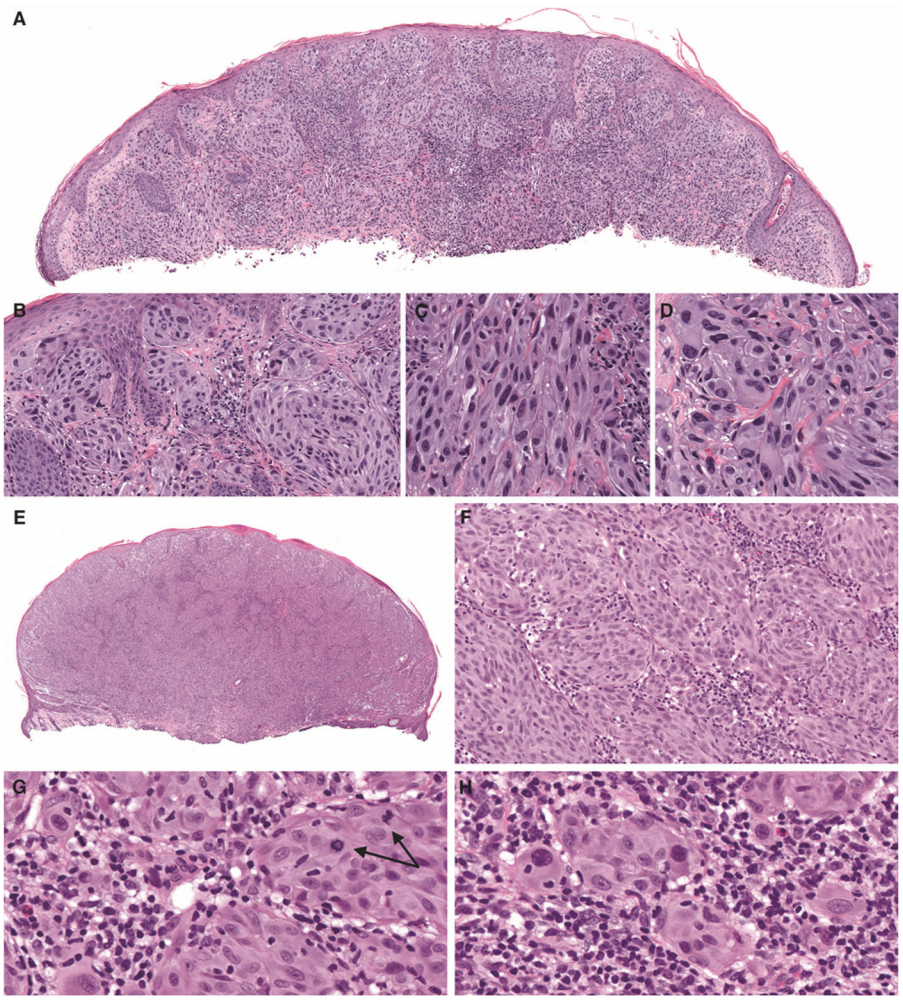

Fig. 2 Spitz melanocytomas (atypical Spitz tumors) with *ETV6*-NTRK3 fusion. a Low-power view shows a domed-shaped tumor (case 7). **b** There is epidermal hyperplasia and a junctional component. **c** In some areas, melanocytes are elongated with ground-glass cytoplasm. **d** In other areas, melanocytes are epithelioid with distinct cell borders and pleomorphic, eccentrically placed nuclei. **e** Low-power view shows an exophytic nodule with thinned and focally ulcerated epidermis, and an epidermal collarette (case 4). **f** Large nests of melanocytes are present with an associated permeative lymphocytic infiltrate. **g** Dermal mitoses deep within the tumor are easily identified (arrows). **h** Some melanocytes contain lymphocytes within their cytoplasm.

Melanocytic tumors with *MYO5A-NTRK3* fusion often demonstrated a fascicular growth pattern which was occasionally plexiform or syncytial (Figs. 3 and 4). In more than half of the *MYO5A-NTRK3* cases, interlacing fascicles were composed of fusiform to spindled melanocytes (62% of cases, compared to 14% in *ETV6-NTRK3* and none of the *MYH9-NTRK3* tumors), which gave the tumors a neuroid appearance. Another characteristic feature, detected exclusively in tumors with *MYO5A-NTRK3* fusions, was palisading of the nuclei with the formation of pseudo-Verocay bodies or pseudo-rosettes, which additionally contributed to the neuroid appearance of these tumors (Figs. 2 and 4). Large epithelioid melanocytes as a minor population within a background of spindled melanocytes were observed only in two tumors with *MYO5A-NTRK3* fusions, both melanomas (Fig. 4).

Both cases harboring the *MYH9-NTRK3* fusion (Fig. 5) were dermal nodules embedded in a prominently fibrotic stroma. In one of the tumors there was collagen trapping at periphery and "honeycomb" pattern of infiltration into the fat. In another case, there was lateral displacement of the elastotic material by the desmoplastic melanocytic tumor. Cells were epithelioid, arranged syncytially, or in small aggregates placed between coarsened collagen bundles. Mitoses were not identified.

ETV6-NTRK3 and MYO5A-NTRK3 have distinct locations within melanocytes and result in different phenotypic changes

Antibodies that recognize the kinase domain of NTRK3 are known to demonstrate nuclear positivity in tumors with *ETV6-NTRK3* fusions, suggesting that the fusion protein localizes to the nucleus. ETV6 is an ETS family transcription factor that is localized predominantly to the nucleus; this localization depends on its nuclear localization motif located within residues 332–452 [31]. *ETV6-NTRK3* fusions characteristically contain only exons 1–5 of ETV6, which do not encode the nuclear localization motif of ETV6. It has been recently demonstrated that the cytoplasmic portion of NTRK3 contains a nuclear localization signal within the kinase domain that results in nuclear

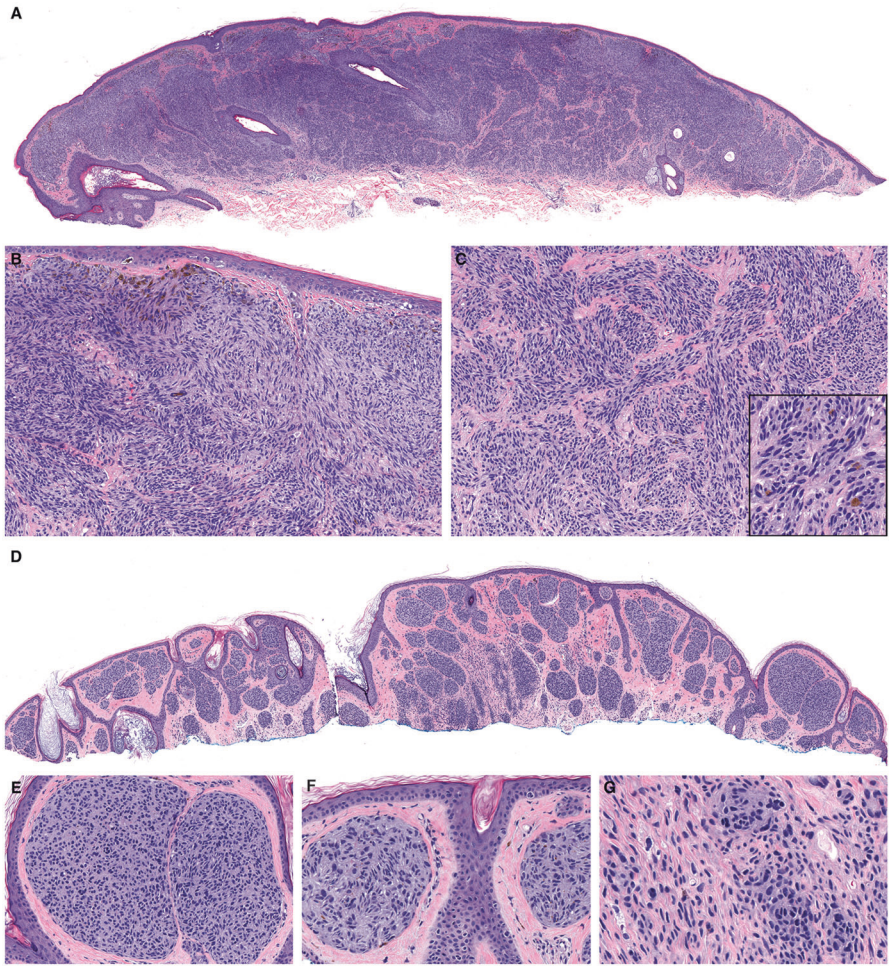

Fig. 3 Melanocytic tumors with *MYO5A-NTRK3* fusion display unique histopathologic features. a Case 10 is a broad, dome-shaped predominantly intradermal tumor. **b** The constituent melanocytes are monomorphous and spindled throughout with a fascicular to plexiform growth pattern that occasionally show palisading resembling Verocay bodies. Marked pigmentation of some superficial melanocytes is present. **c** Within the dermis, nests of spindled melanocytes are present in fascicular nests and focal pigmentation is present (inset). **d** Case 18 has a similar profile from low-power. **e** Large nests of melanocytes with small hyperchromatic nuclei are present in the papillary dermis beneath a thinned epidermis. **f** Pseudo-rosettes are present within nests of melanocytes. **g** In the deep portion, elongated melanocytes are dispersed as small nests and single melanocytes.

translocation of fragments of NTRK3 generated by caspase cleavage [32]. This nuclear localization signal of NTRK3 is retained in both ETV6-NTRK3 and MYO5A-NTRK3 fusion proteins.

MYO5A is a processive actin-based motor that is involved in melanosome transport to the dendrites of melanocytes [33]. MYO5A has four distinct regions: the N-terminal motor domain, a neck domain with binding sites for light chains, a proximal tail domain that contains coiled-coil domains that lead to dimerization and a C-terminal globular tail domain that inhibits the motor domain unless bound to cargo [34]. MYO5A-NTRK3 fusion proteins contain the first three regions with variable numbers of coiled–coiled domains but lack the C-terminal globular tail domain. Thus, MYO5A-NTRK3 proteins would be predicted to dimerize and travel along actin filaments without the ability of binding to cargo.

To further characterize these two fusion proteins, we lentivirally transduced immortalized mouse melanocytes to express ETV6-NTRK3 or MYO5A-NTRK3 each with a V5 tag at the C-terminus (Fig. 6a, b). The expression of both fusion proteins resulted in increased levels of phosphorylated ERK and AKT as compared to GFP transduced controls. While the amount of MYO5A-NTRK3 expressed appeared significantly lower than the amount of ETV6-NTRK3 expressed as assessed by Western blotting for the V5 epitope, the levels of phosphorylated ERK and AKT were similar, indicating that MYO5A-NTRK3 more strongly activates the MAPK and PI3K pathways. Melanocytes expressing ETV6-NTRK3-V5 adopted a rounded, flattened cytomorphology whereas those expressing MYO5A-NTRK3-V5 adopted a highly dendritic cytomorphology. We visualized the subcellular localization of the two distinct NTRK3 fusion proteins by immunofluorescence using an anti-V5 primary antibody. ETV6-NTRK3-V5 was diffusely localized both to the nucleus and the cytoplasm with increased concentration in the nucleus. In contrast, MYO5A-NTRK3-V5 levels were increased within dendrites as compared to the cell body and appeared excluded from the nucleus (Fig. 6c).

This distinct localization of the ETV6-NTRK3 and MYO5A-NTRK3 fusion proteins was reflected in melanocytic tumors from patients. Immunohistochemistry using a pan-TRK antibody that recognizes the kinase domain of Trk

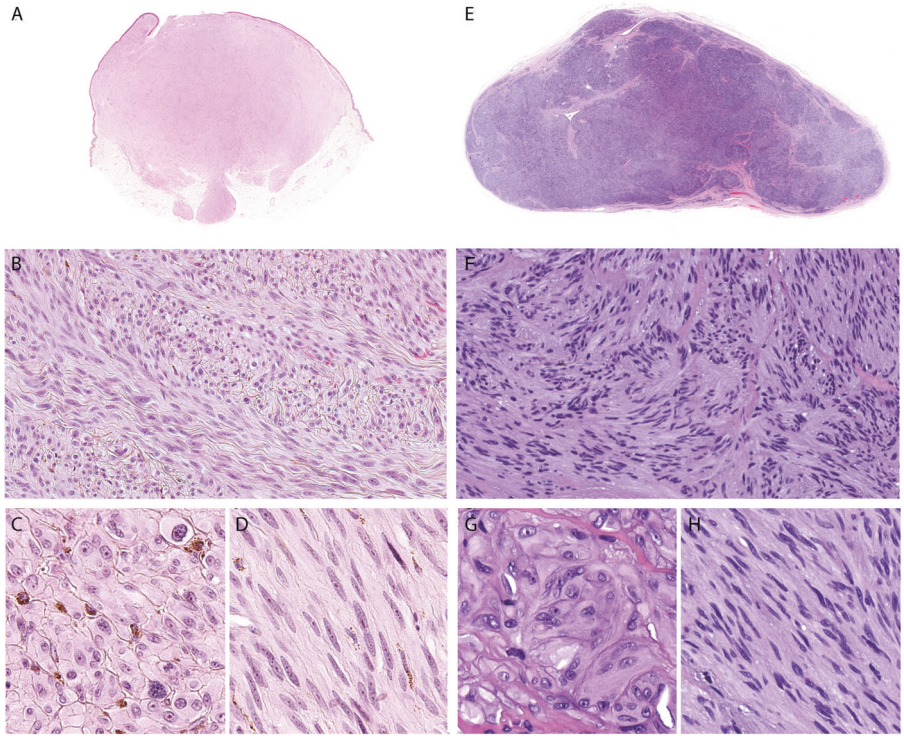

Fig. 4 Melanomas with *MYO5A-NTRK3* fusion demonstrate nodules of spindled melanocytes with a fascicular growth pattern and areas of marked cytologic atypia. a Low-power view of case 21 shows an exophytic, dermal nodule with bulbous base. **b** Spindled melanocytes are arrayed in densely packed interlacing fascicles. **c** In the superficial portion, dermal melanocytes are epithelioid with distinct cellular membranes, nuclear pleomorphism, and prominent nucleoli. Pigmentation is present within superficial melanocytes. **d** Spindled melanocytes demonstrate visible nucleoli and occasionally contain pigment granules in their fibrillar cytoplasm. **e** Low-power view of case 20 shows a dermal-subcutaneous nodule with multi-lobulated, plexiform pattern, **f** Spindled melanocytes form pseudo-Verocay bodies. **g** In central areas, epithelioid melanocytes with distinct cellular membranes and moderate amounts of ground-glass cytoplasm are arrayed as nests. **h** Spindled melanocytes arranged in fascicles display fibrillar cytoplasm.

proteins (NTRK1/2/3) demonstrated moderate cytoplasmic and intense nuclear positivity in tumors with ETV6-NTRK3 fusion. In contrast, tumors with MYO5A-NTRK3 fusion did not demonstrate nuclear positivity but instead thin linear regions of positivity, suggesting localization to dendrites (Fig. 6d).

Discussion

We describe histopathologic features of melanocytic tumors with *NTRK3* fusions and identify distinct features associated with the recurrent 5′ fusion partners *ETV6* and *MYO5A*. *NTRK3* fusions occur in a mutually exclusive pattern with other MAPK activating initiating mutations such as *BRAF* and *NRAS* mutations and other kinase fusions and thus are considered an initiating mutation, which gives rise to a melanocytic nevus. Our study did not include pigmented spindle cell nevi, a category in which others have shown that *NTRK3* fusions are present in over half of cases. This difference is likely due to the fact that our cases were selected from consultations or ambiguous melanocytic neoplasms, and do not reflect an overall survey of melanocytic tumors with *NTRK3* fusion [6]. The majority of the cases in our study were predominantly dermal. It remains to be seen if the histopathologic differences we identified between *ETV6-NTRK3*- and *MYO5A-NTRK3*-fused predominantly dermal melanocytic tumors are also present in melanocytic tumors that are predominantly intraepidermal and may arise from a distinct cell of origin.

Melanocytic tumors with *ETV6-NTRK3* were sometimes reminiscent of *BAP1*-inactivated melanocytomas with nested or sheet-like collections of epithelioid melanocytes with well-defined nuclear membranes, eccentrically placed nuclei, and a permeative lymphocytic infiltrate. However, in contrast to *BAP1*-inactivated melanocytomas, which typically harbor *BRAF* V600E mutations and bi-allelic inactivation of *BAP1* [2, 35], tumors with *ETV6-NTRK3* demonstrated less cellular and nuclear pleomorphism. In about a quarter of cases with *ETV6-NTRK3*, an intraepidermal component was present and this is unusual in *BAP1*-inactivated melanocytomas, outside of those associated with germline *BAP1* mutations [2, 35, 36]. However, a separate component composed of smaller melanocytes, which in

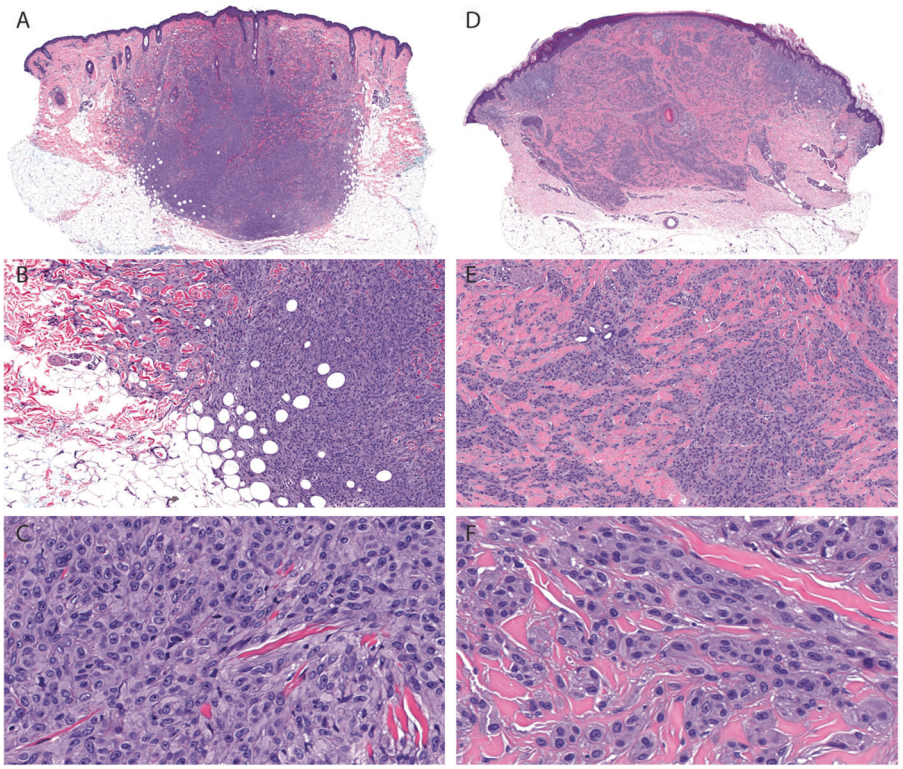

Fig. 5 Architectural and cytologic features of melanocytic tumors with *MYH9-NTRK3* fusion. a At scanning magnification, case 2 is intradermal with a nodular configuration and extends into the subcutis. **b** There is "honeycomb" pattern of infiltration into the subcutis and "collagen trapping" at periphery of the tumor. **c** Constituent melanocytes are moderately large and epithelioid arranged syncytially. **d** Low-power view of case 22 shows an intradermal tumor. Markedly desmoplastic stroma displaces the elastotic material in the superficial dermis. **e** Melanocytes are arrayed as small aggregates and single cells intercalating between thickened collagen bundles. There is infiltrative growth pattern around eccrine glands and arrector pili muscle. **f**. Epithelioid melanocytes have well-defined cellular membranes.

BAP1-inactivated melanocytomas represent the antecedent conventional nevus with intact *BAP1*, was never identified in tumors with *ETV6-NTRK3*. This supports the notion that *ETV6-NTRK3* is sufficient for the formation of a Spitz nevus with epithelioid melanocytes that does not go through a step-wise progression requiring additional genetic alterations.

In contrast, tumors with *MYO5A-NTRK3* were typically composed of spindled rather than epithelioid melanocytes, arrayed in fascicles or nests. While the fascicular arrangement of melanocytes is reminiscent of that seen in *ALK* fused Spitz tumors, the spindled melanocytes in *MYO5A-NTRK3* tumors have thinner and more uniformly staining nuclei. Thus, these tumors often resembled neurotized nevi or neural tumors with melanocytic markers needed to confirm melanocytic lineage in some cases. In contrast to neurotized nevi, however, in tumors with *MYO5A-NTRK3* melanocytes with elongated nuclei were typically present throughout the tumor, rather than being accentuated at the base. While the presence of an *NTRK3* fusion is considered diagnostic of a Spitz tumor according to the 2018 WHO classification of skin tumors, some *MYO5A-NTRK3* tumors would not be recognized as Spitz tumors by histopathologic evaluation alone.

Our study was limited by the fact that we did not perform comprehensive gene panel sequencing of the tumors, only assessment for *NTRK3* fusion (by aCGH or RNA-Seq). While tumors with *ETV6-NTRK3* or *MYO5A-NTRK3* had different patterns of copy number alterations on chromosome 12p (where *ETV6* is located) and chromosome 15q (where *MYO5A* and *NTRK3* are located) other copy number differences were not notable between the tumors with these different *NTRK3* fusions.

The observation that some histopathologic features are predictive of which RTK fusion is present in a Spitz tumor [10–13] is thought to reflect the biologic differences between the RTKs and the different downstream signaling that results. We hypothesized that because tumors with *ETV6-NTRK3* and *MYO5A-NTRK3* have distinct histopathologic features that the fusion proteins would have distinct biologic characteristics. While NTRK3 is a transmembrane protein localized predominantly to the plasma membrane, we found that ETV6-NTRK3 and MYO5A-NTRK3 have distinct subcellular localizations. While both contain the nuclear localization signal of NTRK3, only ETV6-NTRK3 was demonstrated to localize to the nucleus. In contrast, MYO5A-NTRK3 likely binds to and travels along actin filaments as the myosin motor and portions of the dimerization domain of MYO5A are retained in the fusion protein. Melanocytes contain a cortical shell of actin along dendrites, which allows MYO5A and melanosomes to colocalize in the periphery in normal melanocytes [37]. The localization of MYO5A-NTRK3 observed corresponds with localization to this cortical shell of actin, likely anchoring the fusion protein and preventing nuclear import.

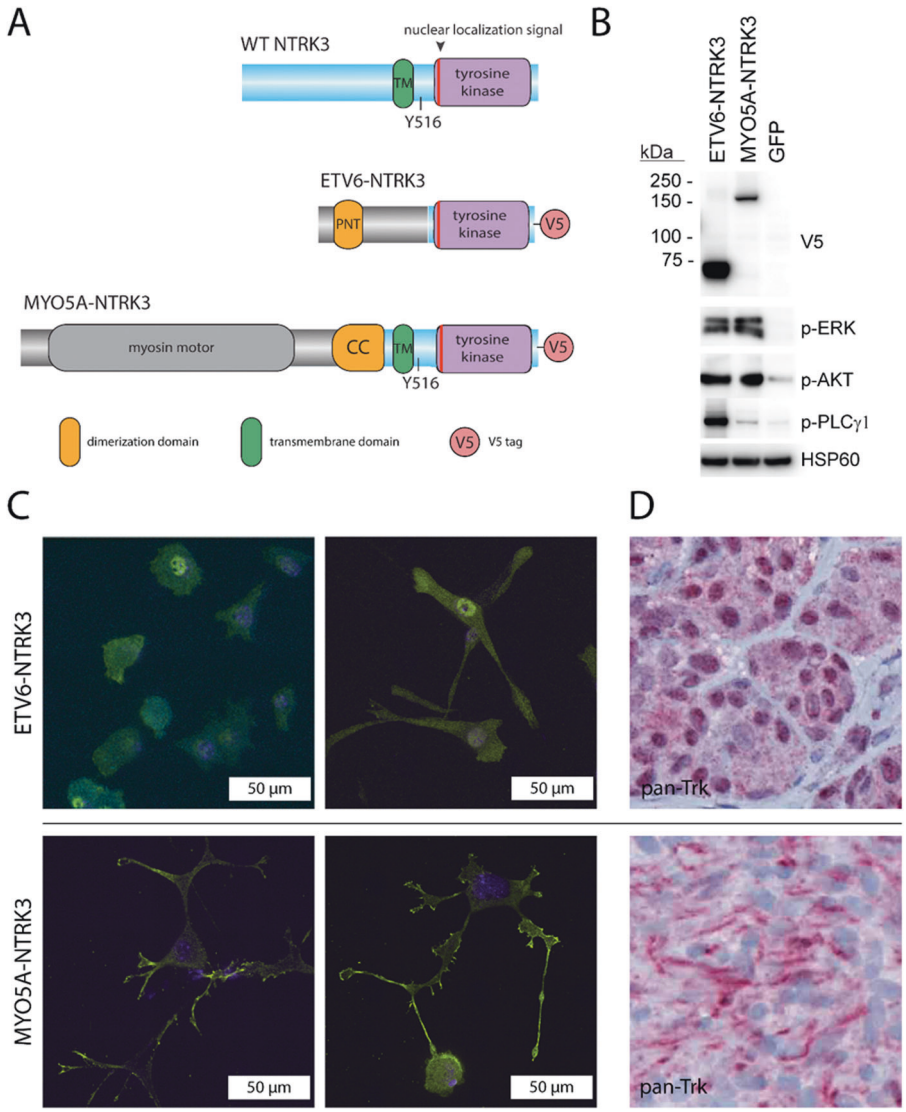

Fig. 6 NTRK3 fusions contain different portions of NTRK3 and have distinct subcellular localizations. a Diagram of protein domains in ETV6-NTRK3-V5 and MYO5A-NTRK3-V5 fusion proteins expressed in melan-a cells as compared to wild-type NTRK3. **b** Western blot of protein lysates from melan-a stably transduced with ETV6-NTRK3-V5, MYO5A-NTRK3-V5 and GFP demonstrates the tagged proteins at the predicted molecular weights. Activation of the MAPK (p-ERK), PI3K (p-AKT), and PLCγ (p- PLCγ) pathways is seen with expression of the fusion proteins as compared to GFP expressing control. **c** ETV6-NTRK3 and MYO5A-NTRK3 have distinct subcellular localizations and confer distinct cytomorphologic features when expressed in melanocytes. The fusion proteins are detected by an anti-V5 antibody conjugated to a Cy3 fluorophore (yellow). DAPI counterstain (blue) highlights the nucleus. In the left column, melan-a cells expressing ETV6-NTRK3 show a more epithelioid morphology with a few thick and short dendritic processes. ETV6-NTRK3 is localized diffusely to the cytoplasm with increased concentration in the nucleus. In the right column, melan-a cells expressing MYO5A-NTRK3 demonstrated a highly dendritic morphology with an increased number of long, thin, and branching dendrites. MYO5A-NTRK3 is localized to the cytoplasm with a lower concentration in the nucleus. The fusion protein is concentrated within the dendrites and at the tips of dendritic processes. **d** In melanocytic tumors from patients, those with *ETV6-NTRK3* demonstrate strong nuclear and moderate cytoplasmic NTRK kinase domain (left) while those with *MYO5A-NTRK3* demonstrate cytoplasmic expression of NTRK kinase with strong linear staining likely along dendritic processes by pan-TRK immunochemistry.

Some RTKs or fragments of them are localized to the nucleus where they have been demonstrated to participate in nuclear MAPK signaling and interact with transcription factors to modulate gene expression [38]. As ETV6-NTRK3 retains the DNA binding domain of ETV6, the fusion protein may regulate transcription when present in the nucleus.

In addition, ETV6-NTRK3 and MYO5A-NTRK3 contain different portions of NTRK3. ETV6-NTRK3 does not contain tyrosine 516 of NTRK3, which is phosphorylated after activation to create a docking site for Shc, fibroblast growth factor receptor substrate 2, the p85 subunit of PI3K, and other adapters, which lead to activation of the Ras and

PI3K pathways [14]. The absence of this docking site in ETV6-NTRK3 results in its dependence on binding to insulin-like growth factor 1 receptor (IGF1R) and insulin receptor substrate 1 (IRS1) to activate PI3K and transform cells [39, 40]. As MYO5A-NTRK3 does contain tyrosine 516 of NTRK3, dependence on binding to IGF1R and IRS1 would not be expected.

In vitro, MYO5A-NTRK3 but not ETV6-NTRK3 induced dendritic outgrowth and branching in melanocytes, echoing the known role of NTRK3 signaling in dendrite morphogenesis during neuronal development [41]. Perhaps the NTRK3 signaling that induces such dendritic outgrowth occurs through adapter proteins that bind to tyrosine 516 of NTRK3, accounting for the lack of induced dendritic outgrowth with expression of ETV6-NTRK3.

This is the first study to note phenotypic differences in melanocytic tumors based on the 5′ partner of the *NTRK3* fusion. The nature of the 5′ partner gene also affects the biological function of *BRAF* fusions and can impact the response to RAF inhibitors [42]. Here, our work indicates that differences in subcellular localization and functional portions of the kinase included in the fusion protein are additional factors that may affect biologic function and potentially response to TRK inhibitor therapy.

Funding SP was supported by a grant from the European Academy of Dermatology and Venereology (RF-2017-17). This work was supported by the National Cancer Institute at the National Institutes of Health (Grant Number 1R35CA220481). Immunofluorescence imaging was done at the Nikon Imaging Center, UCSF.

Compliance with ethical standards

Conflict of interest The authors declare that they have no conflict of interest.

Publisher's note Springer Nature remains neutral with regard to jurisdictional claims in published maps and institutional affiliations.

References

1. Schram AM, Chang MT, Jonsson P, Drilon A. Fusions in solid tumours: diagnostic strategies, targeted therapy, and acquired resistance. Nat Rev Clin Oncol. 2017;14:735–48.
2. Wiesner T, Murali R, Fried I, Cerroni L, Busam K, Kutzner H, et al. A distinct subset of atypical spitz tumors is characterized by BRAF mutation and loss of BAP1 expression. Am J Surg Pathol. 2012;36:818–30.
3. Yeh I, Botton T, Talevich E, Shain AH, Sparatta AJ, de la Fouchardiere A, et al. Activating MET kinase rearrangements in melanoma and Spitz tumours. Nat Commun. 2015;6:7174.
4. Yeh I, Tee MK, Botton T, Shain AH, Sparatta AJ, Gagnon A, et al. NTRK3 kinase fusions in Spitz tumours. J Pathol. 2016;240:282–90.
5. Wang L, Busam KJ, Benayed R, Cimera R, Wang J, Denley R, et al. Identification of NTRK3 Fusions in Childhood Melanocytic Neoplasms. J Mol Diagn. 2017;19:387–96.
6. VandenBoom T, Quan VL, Zhang B, Garfield EM, Kong BY, Isales MC, et al. Genomic fusions in pigmented spindle cell nevus of reed. Am J Surg Pathol. 2018;42:1042–51.
7. Pollock PM, Harper UL, Hansen KS, Yudt LM, Stark M, Robbins CM, et al. High frequency of BRAF mutations in nevi. Nat Genet. 2003;33:19–20.
8. Yeh I, von Deimling A, Bastian BC. Clonal BRAF mutations in melanocytic nevi and initiating role of BRAF in melanocytic neoplasia. J Natl Cancer Inst. 2013;105:917–9.
9. Elder DE, Massi D, Scolyer R, Willemze R. WHO classification of skin tumours, 4th ed. Lyon, France: IARC Press; 2018.
10. Busam KJ, Kutzner H, Cerroni L, Wiesner T. Clinical and pathologic findings of Spitz nevi and atypical Spitz tumors with ALK fusions. Am J Surg Pathol. 2014;38:925–33.
11. Yeh I, de la Fouchardiere A, Pissaloux D, Mully TW, Garrido MC, Vemula SS, et al. Clinical, histopathologic, and genomic features of Spitz tumors with ALK fusions. Am J Surg Pathol. 2015;39:581–91.
12. Amin SM, Haugh AM, Lee CY, Zhang B, Bubley JA, Merkel EA, et al. A comparison of morphologic and molecular features of BRAF, ALK, and NTRK1 fusion spitzoid neoplasms. Am J Surg Pathol. 2017;41:491–8.
13. Yeh I, Busam KJ, McCalmont TH, LeBoit PE, Pissaloux D, Alberti L, et al. Filigree-like rete ridges, lobulated nests, rosette-like structures, and exaggerated maturation characterize spitz tumors with NTRK1 fusion. Am J Surg Pathol. 2019;43:737–46.
14. Huang EJ, Reichardt LF. Trk receptors: roles in neuronal signal transduction*. Annu Rev Biochem. 2003;72:609–42.
15. Yaar M, Eller MS, DiBenedetto P, Reenstra WR, Zhai S, McQuaid T, et al. The trk family of receptors mediates nerve growth factor and neurotrophin-3 effects in melanocytes. J Clin Invest. 1994;94:1550–62.
16. Tognon C, Knezevich SR, Huntsman D, Roskelley CD, Melnyk N, Mathers JA, et al. Expression of the ETV6-NTRK3 gene fusion as a primary event in human secretory breast carcinoma. Cancer Cell. 2002;2:367–76.
17. Skálová A, Vanecek T, Sima R, Laco J, Weinreb I, Perez-Ordonez B, et al. Mammary analogue secretory carcinoma of salivary glands, containing the ETV6-NTRK3 fusion gene: a hitherto undescribed salivary gland tumor entity. Am J Surg Pathol. 2010;34:599–608.
18. Del Castillo M, Chibon F, Arnould L, Croce S, Ribeiro A, Perot G, et al. Secretory breast carcinoma: a histopathologic and genomic spectrum characterized by a joint specific ETV6-NTRK3 gene fusion. Am J Surg Pathol. 2015;39:1458–67.
19. Church AJ, Calicchio ML, Nardi V, Skalova A, Pinto A, Dillon DA, et al. Recurrent EML4-NTRK3 fusions in infantile fibrosarcoma and congenital mesoblastic nephroma suggest a revised testing strategy. Mod Pathol Off J U S Can Acad Pathol Inc. 2018;31:463–73.
20. Gatalica Z, Xiu J, Swensen J, Vranic S. Molecular characterization of cancers with NTRK gene fusions. Mod Pathol Off J U S Can Acad Pathol Inc. 2019;32:147–53.
21. Farago AF, Taylor MS, Doebele RC, Zhu VW, Kummar S, Spira AI, et al. Clinicopathologic features of non-small-cell lung cancer harboring an NTRK gene fusion. JCO Precis Oncol. 2018;2018. https://doi.org/10.1200/PO.18.00037.
22. Yakushina VD, Lerner LV, Lavrov AV. Gene fusions in thyroid cancer. Thyroid. 2017;28:158–67.
23. Chiang S, Cotzia P, Hyman DM, Drilon A, Tap WD, Zhang L, et al. NTRK fusions define a novel uterine sarcoma subtype with features of fibrosarcoma. Am J Surg Pathol. 2018;42:791–8.
24. Robinson CL, Evans RD, Sivarasa K, Ramalho JS, Briggs DA, Hume AN. The adaptor protein melanophilin regulates dynamic myosin-Va:cargo interaction and dendrite development in melanocytes. Mol Biol Cell. 2019;30:742–52.

25. Pastural E, Barrat FJ, Dufourcq-Lagelouse R, Certain S, Sanal O, Jabado N, et al. Griscelli disease maps to chromosome 15q21 and is associated with mutations in the myosin-Va gene. Nat Genet. 1997;16:289–92.
26. Dobin A, Davis CA, Schlesinger F, Drenkow J, Zaleski C, Jha S, et al. STAR: ultrafast universal RNA-seq aligner. Bioinformatics. 2013;29:15–21.
27. Kim D, Pertea G, Trapnell C, Pimentel H, Kelley R, Salzberg SL. TopHat2: accurate alignment of transcriptomes in the presence of insertions, deletions and gene fusions. Genome Biol. 2013;14: R36.
28. Chen X, Schulz-Trieglaff O, Shaw R, Barnes B, Schlesinger F, Källberg M, et al. Manta: rapid detection of structural variants and indels for germline and cancer sequencing applications. Bioinformatics. 2016;32:1220–2.
29. Bennett DC, Cooper PJ, Hart IR. A line of non-tumorigenic mouse melanocytes, syngeneic with the B16 melanoma and requiring a tumour promoter for growth. Int J Cancer. 1987;39:414–8.
30. Korbel JO, Campbell PJ. Criteria for inference of chromothripsis in cancer genomes. Cell. 2013;152:1226–36.
31. Park H, Seo Y, Kim JI, Kim W, Choe SY. Identification of the nuclear localization motif in the ETV6 (TEL) protein. Cancer Genet Cytogenet. 2006;167:117–21.
32. Ménard M, Costechareyre C, Ichim G, Blachier J, Neves D, Jarrosson-Wuilleme L, et al. Hey1- and p53-dependent TrkC proapoptotic activity controls neuroblastoma growth. PLoS Biol. 2018;16:e2002912.
33. Mehta AD, Rock RS, Rief M, Spudich JA, Mooseker MS, Cheney RE. Myosin-V is a processive actin-based motor. Nature. 1999;400:590–3.
34. Trybus KM. Myosin V from head to tail. Cell Mol Life Sci CMLS. 2008;65:1378–89.
35. Yeh I, Mully TW, Wiesner T, Vemula SS, Mirza SA, Sparatta AJ, et al. Ambiguous melanocytic tumors with loss of 3p21. Am J Surg Pathol. 2014;38:1088–95.
36. Busam KJ, Sung J, Wiesner T, von Deimling A, Jungbluth A. Combined BRAF(V600E)-positive melanocytic lesions with large epithelioid cells lacking BAP1 expression and conventional nevomelanocytes. Am J Surg Pathol. 2013;37:193–9.
37. Wu X, Bowers B, Rao K, Wei Q, Hammer JA. Visualization of melanosome dynamics within wild-type and dilute melanocytes suggests a paradigm for myosin V function in vivo. J Cell Biol. 1998;143:1899–918.
38. Schlessinger J, Lemmon MA. Nuclear signaling by receptor tyrosine kinases: the first robin of spring. Cell. 2006;127:45–8.
39. Lannon CL, Martin MJ, Tognon CE, Jin W, Kim S-J, Sorensen PHB. A highly conserved NTRK3 C-terminal sequence in the ETV6-NTRK3 oncoprotein binds the phosphotyrosine binding domain of insulin receptor substrate-1: an essential interaction for transformation. J Biol Chem. 2004;279:6225–34.
40. Tognon CE, Martin MJ, Moradian A, Trigo G, Rotblat B, Cheng S-WG, et al. A tripartite complex composed of ETV6-NTRK3, IRS1 and IGF1R is required for ETV6-NTRK3-mediated membrane localization and transformation. Oncogene. 2012;31:1334–40.
41. Joo W, Hippenmeyer S, Luo L. Neurodevelopment. Dendrite morphogenesis depends on relative levels of NT-3/TrkC signaling. Science. 2014;346:626–9.
42. Botton T, Talevich E, Mishra VK, Zhang T, Shain AH, Berquet C, et al. Genetic heterogeneity of BRAF fusion kinases in melanoma affects drug responses. Cell Rep. 2019;29:573–88.e7.